

Investigation of the two-dimensional electron gas in HgCdTe by quantum Hall effect measurements

W. P. Kirk and P. S. Kobiela

Physics Department, Texas A&M University, College Station, Texas 77843

R. A. Schiebel and M. A. Reed

Central Research Laboratories, Texas Instruments, Inc., Dallas, Texas 75265

(Received 15 December 1985; accepted 10 March 1986)

By means of the first observations of the quantum Hall effect in a type II-VI semiconducting compound, $\text{Hg}_{1-x}\text{Cd}_x\text{Te}$, we have studied the two-dimensional electron gas formed by the inversion layer of a MISFET (metal-insulator-semiconductor field effect transistor) device. Extensive details regarding the fabrication and use of the MISFET are described. The data also indicate an abrupt onset of the quantum Hall effect which, when interpreted with a percolation threshold theory, is used to further investigate conditions affecting charge transport mechanisms in the two-dimensional electron gas at a HgCdTe interface.

I. INTRODUCTION

The quantum Hall effect (QHE)¹ is a low temperature effect, occurring in a two-dimensional electron gas (2-DEG), characterized by the quantization of the Hall resistance in coincidence with a vanishing resistivity parallel to the current. The 2-DEG may be produced by a MOSFET structure,¹ or by an MBE-grown heterostructure² or superlattice.³ The effect is sensitive to interface properties as well as epitaxial growth conditions, and is of interest in the characterization of inversion layers, heterostructures, and superlattices. To date, the QHE effect has been demonstrated only in silicon and III-V structures. Here we report on the first demonstration of the QHE in HgCdTe (MCT) where the 2-DEG is formed in the inversion layer of a MISFET (metal-insulator-semiconductor field effect transistor) device.

For a pure two-dimensional noninteracting electron gas in a perpendicular magnetic field, the Hall and longitudinal conductivities, σ_{xy} and σ_{xx} , can be calculated exactly provided that an integral number of Landau levels are precisely filled. Each filled level has a density given by $n_0 = eB/h$. This situation holds under conditions of large magnetic field B and very low temperatures T such that $\hbar\omega_c \gg kT$, where $\omega_c = eB/m^*$ is the cyclotron frequency. When these unique conditions are fulfilled, the charge carriers cannot undergo dissipative scattering because the energy gap formed by the Landau levels prevents state changes. The result, then, is that the diagonal resistivity vanishes, i.e., $\rho_{xx} = 0$. Since $\sigma_{xx} = \rho_{xx}/(\rho_{xy}^2 + \rho_{xx}^2)$, then $\sigma_{xx} = 0$ as well, and the charges simply drift perpendicular to the applied electric and magnetic fields. The resulting Hall conductivity is given by $\sigma_{xy} = ne/B = in_0e/B = ie^2/h$, where i is the (integral) number of filled Landau levels. A matrix inversion yields $\rho_{xy} = \sigma_{xy}/(\sigma_{xy}^2 + \sigma_{xx}^2) = h/ie^2$, which is the Hall resistance quantized in units of $25\,813\,\Omega$.

Surprisingly, one finds that in actual experiments on inversion layers, at sufficiently strong fields, low temperatures, and high mobilities, the values of ρ_{xx} and ρ_{xy} agree with the above ideal values to an astonishing precision. Furthermore, these values persist over a finite interval as the density (a function of applied gate voltage in FET devices) or the mag-

netic field is varied. The result is a step structure in the Hall resistivity versus gate voltage or field. The plateau regions in the Hall resistivity cannot be explained without invoking localized states in which some of the available electrons are localized by the random scattering potentials that were created at the interface due to the surface conditions of the substrate. The remaining subset of electrons, referred to as extended states, are available to carry the current in the inversion layer. These extended state electrons can also be thought of as forming a type of fluid with effectively the ideal (perfect Landau-level) density. However, without the localized states, the Fermi energy could never be established at values between the Landau levels and, therefore, the characteristic plateau regions in ρ_{xy} and the dissipationless regions in ρ_{xx} would never appear.

Hence, an additional purpose of this paper is to show the interrelationship between localized states and extended states in the quantum Hall effect and thereby gain additional details about the charge transport processes in a two-dimensional electron gas. Currently, the number of ways to probe a 2-DEG is very restricted; therefore any useful information gained along these lines is quite welcomed. We will present data that clearly demonstrate a percolation threshold of the extended states in the quantum Hall regime, and in turn use this observation to obtain quantitative values for the density of effective scattering centers.

II. EXPERIMENTAL PROCEDURES

A. MCT sample structure and fabrication

The MCT sample is a long wavelength n -channel $\text{Hg}_{1-x}\text{Cd}_x\text{Te}$ MISFET device. It was fabricated on single crystal p -type HgCdTe, grown by the solid state recrystallization technique.⁴ From high frequency CV measurements on independent MIS gates, the hole concentration was determined to be about $3 \times 10^{15}\text{ cm}^{-3}$. Spectral response measurements performed on a diode at 77 K show the cutoff wavelength to be $9.7\,\mu\text{m}$. This corresponds to an x value of 0.22 and a band gap of 0.127 eV.

Figure 1 depicts a top view of the device showing the geometry of the contacts for making transport measurements.

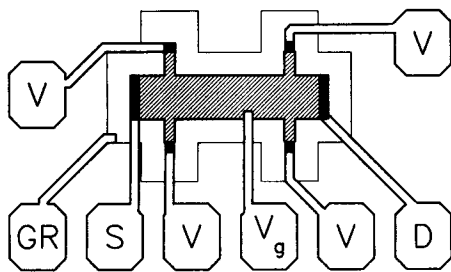


FIG. 1. Top view of MISFET device. Darkened areas, ■, show ion-implanted regions. S = source, D = drain, GR = guard ring, V_g = gate (Hall bar shape, section lined), V = longitudinal potential V_{xx} , and Hall potential V_{xy} , probes.

This device incorporates two independently functioning metal gate levels, fabricated on two different insulator thicknesses above the *p*-type HgCdTe substrate, as shown in the side view of Fig. 2. Both of these gates are used to control the HgCdTe surface potential. The central gate, in the shape of a Hall bar ($w = 107 \mu\text{m}$, $l = 406 \mu\text{m}$), is used to form an inversion layer at the HgCdTe surface. The other peripheral gate (guard ring) is used to control the surface potential on the periphery of the Hall geometry and to eliminate unwanted surface channels or inversion layers outside the limits of the Hall geometry. Contact is made to the inversion layer through the use of *n*-type diode regions formed at the extremities (i.e., at the source, drain, and potential probes) of the Hall geometry by ion implantation. By applying appropriate potentials to the Hall gate, it was possible to vary the charge-carrier density between $n = 1.36 \times 10^{11}$ and $5.32 \times 10^{11} \text{ cm}^{-2}$; correspondingly, the mobility changed from $\mu = 6.28 \times 10^4 \text{ cm}^2/\text{V s}$ to $\mu = 4.89 \times 10^4 \text{ cm}^2/\text{V s}$, at $T < 1 \text{ K}$.

Diodes were formed by room temperature ion implantation of boron at 100 keV with a 10^{13} cm^{-2} dose. The *n*-type conversion is assumed to be due to the donorlike implant damage.⁵ No intentional anneals were performed on the samples. As shown in Fig. 2, the gate insulators were 800 Å of native (anodic) oxide followed by 2000 Å of ZnS under the Hall gate. Another 4500 Å of ZnS was used for the upper insulator level under the guard ring. The floating metal gates were deposited by resistive boat evaporation of aluminum or nickel. Bond pads were made by evaporation of indium, and electrical contacts were made from the pads to the device elements by etched vias.

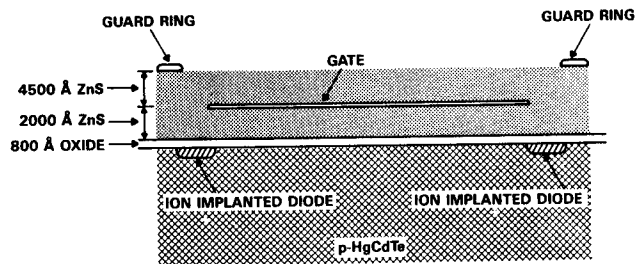


FIG. 2. Side view of MISFET (cross sectioned from source to drain) showing insulator thickness and floating gate locations.

B. Biasing

In the following discussion, the HgCdTe substrate is assumed to be grounded. Because of a positive fixed charge at the HgCdTe-insulator interface, the HgCdTe surface is inverted even when no bias is applied to either of the gates. To prevent unwanted surface channels, the guard ring must therefore be biased to flatband (i.e., no energy band bending near the surface). The flatband voltage is determined by the amount of fixed positive charge at the interface as well as by the insulator thickness under the particular gate in question. For the guard ring, this has been found experimentally to be -18.4 V at room temperature and -19.1 V at 4.2 K.

For the Hall gate, the flatband voltage V_{fb} was measured to be -6.3 V . The threshold voltage V_{th} for this gate, defined as the voltage that produces a surface potential of twice the Fermi potential, was found to be -5.8 V . Biases more negative than V_{fb} will tend to accumulate the surface, biases greater than V_{th} will more strongly invert the surface, and intermediate biases will deplete or weakly invert the surface. Additional details concerning *n*-channel MISFET's similar to the construction and behavior of this device are described elsewhere.⁶

C. Radiation exposure

We found certain characteristic parameters of the MCT, especially at low temperatures, to be greatly influenced by the amount of exposure the device experienced from electromagnetic radiation coming from ordinary room lighting. Flatband voltages of the gate and the guard ring are UV sensitive. Normal background lighting will not appreciably alter the flatband voltage, but intense light (such as microscope lamps) can cause significant (positive) shifts in the flatband voltage. Most of the UV will anneal out if the device is left to sit in dark conditions overnight at room temperature; all of the UV effect generally anneals out if the device is left to sit in the dark at room temperature for 2 weeks. Therefore, before the start of each cool down, after mounting an MCT sample into the cryostat, we allowed it to sit in the dark, under vacuum, at room temperature for typically 48 to 60 h.

D. GaAs/AlGaAs heterostructure sample

For purposes of making a direct comparison with the MCT sample, we also studied a GaAs/AlGaAs sample. This sample was a modulation doped GaAs/Al_{0.3}Ga_{0.7}As heterostructure grown by MBE on a Cr-doped GaAs substrate. It consisted of 1 μm undoped GaAs, a 150 Å Al_{0.3}Ga_{0.7}As spacer layer, and 500 Å of Si-doped Al_{0.3}Ga_{0.7}As. Fabrication was similar to that of other workers.² The mobility and carrier density, at $T < 1 \text{ K}$, were $\mu = 1.9 \times 10^5 \text{ cm}^2/\text{V s}$ and $n = 3.2 \times 10^{11} \text{ cm}^{-2}$, respectively.

E. Measurement technique

All the samples were mounted in ceramic styled flatpacks so that they could be conveniently plugged into a cold-plate finger, which was well attached thermally to the mixing chamber of a ³He-⁴He dilution refrigerator. The finger design also held the samples in the central field region of the

bore of a superconducting solenoid. All the leads to the samples were constructed as twisted pairs to reduce induced emfs. The leads were, also, thermally anchored to various thermal stages of the cryostat to minimize heat conduction to the sample, and reduce thermal emfs. The measurements were made over a temperature range between 20 mK and 7.0 K, and temperatures were measured using a ³He melting curve thermometer. Magnetic fields, up to 7.8 T, were applied perpendicular to the current.

Figure 3 shows a schematic layout of the electronics used to record data digitally and to control parts of the experimental apparatus using a DEC LSI 11/23 computer. Excitation currents to the sample were applied as square pulses of dc with amplitudes ranging from 10 nA to 5 μA. Both positive and negative polarities were used. A typical pulse sequence consisted of a positive polarity current for 650 ms, followed by a 5 ms switch-off period and then a negative going pulse for 650 ms. After 500 ms of settling time from the beginning of a plus or minus pulse, the digital voltmeters sampled and averaged the voltages for a period of 150 ms. In this way all voltages were recorded simultaneously. Voltages corresponding to each value of plus and minus current were subtracted to eliminate thermal emfs and then saved to memory for further data processing. This pulse sequence was repeated after 5 to 30 s depending on the temperature range and the amount of Joule heating that a given repetition rate might cause. The Hall resistivity ρ_{xy} was then computed simply by dividing the Hall voltage V_{xy} by the excitation current, while the diagonal magnetoresistivity ρ_{xx} was computed from the longitudinal voltage V_{xx} in a similar way.

III. RESULTS AND DISCUSSION

Quantum Hall resistance plateaus ρ_{xy} , corresponding to Landau level filling factors $i = 1$ to 5, have been observed in the MCT sample near 20 mK. Although some of the broader plateaus remained discernible at temperatures as high as 5.8 K, we obtained the highest quality data, i.e., showing sharper features, in the lower millikelvin range. Figure 4(a) shows the behavior of ρ_{xy} versus the magnetic field B at 20

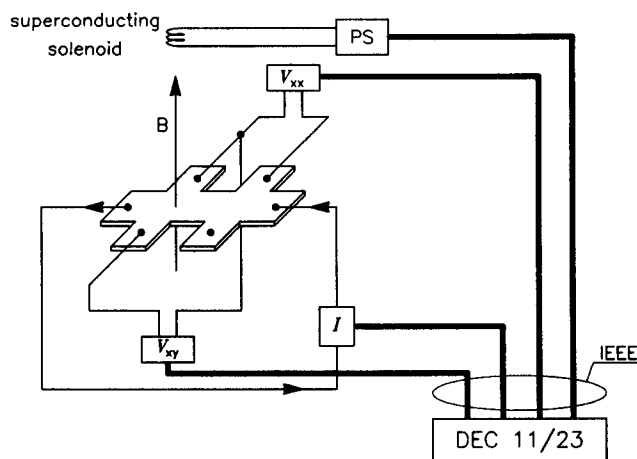


FIG. 3. Schematic of electronic interconnections to the Hall shaped MCT sample. V_{xx} and V_{xy} represent digital voltmeters, I excitation current source, and PS power supply for superconducting solenoid to produce magnetic field B . Instruments connected by IEEE interface to computer.

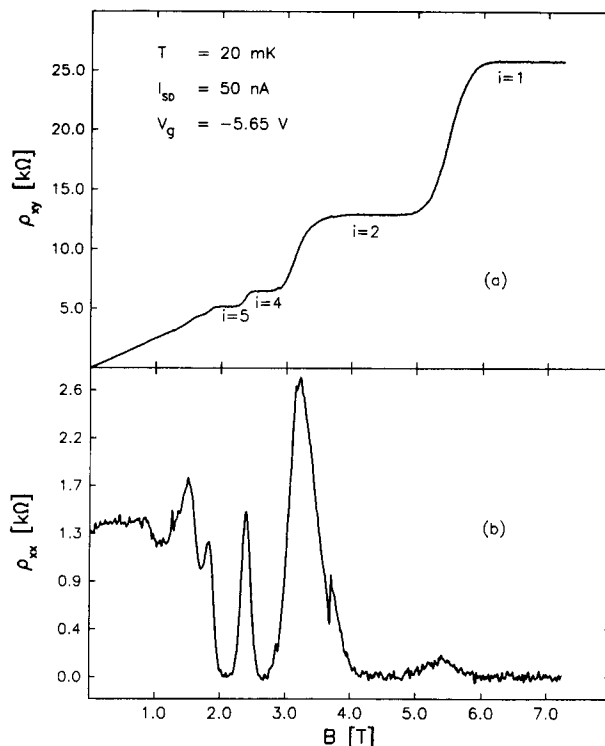


FIG. 4. (a) Hall resistance ρ_{xy} vs magnetic field B for MCT sample with $n = 2.5 \times 10^{11} \text{ cm}^{-2}$. Plateaus labeled with appropriate Landau filling factor, i . (b) Diagonal magnetoresistance ρ_{xx} vs B for MCT at 20 mK.

mK for a carrier density of $2.5 \times 10^{11} \text{ cm}^{-2}$. In this figure the level corresponding to $i = 3$ is missing, however, at higher carrier densities we observe a level corresponding to $i = 3$, but this plateau is never well developed. An example of the behavior of the diagonal magnetoresistance ρ_{xx} as a function of B is shown in Fig. 4(b) for $T = 20 \text{ mK}$. Higher temperature results show similar behavior, but the Shubnikov-de Haas oscillations are less developed due to thermal activation. In Fig. 5 we show the behavior of ρ_{xy} and ρ_{xx} when the gate voltage has been adjusted to give a lower current density, viz., $n = 2.0 \times 10^{11} \text{ cm}^{-2}$, than for the data shown in Fig. 4. At lower fields ($B < 2 \text{ T}$) there is a striking absence of plateaus in ρ_{xy} and the corresponding $\rho_{xx} = 0$ minima. By studying ρ_{xy} and ρ_{xx} for a systematic series of carrier densities, we have determined that below a critical field of $B_c = 2 \text{ T}$ the QHE no longer exists. We believe that this represents the first direct observation of an abrupt onset of the QHE in any known material system. Furthermore, this observation can be interpreted as evidence that the extended states achieve a percolation threshold through the bound scattering centers in a 2-DEG⁷ when $B > B_c$. Joynt and Prange⁸ have shown that when an extended state electron encounters a scattering center, its wave packet will undergo distortion, suffering additive phase shifts, and experience some acceleration to make up for the loss in current due to scattering. This will only happen, however, when the magnetic length, $l = \sqrt{\hbar/eB}$, associated with an extended state wave function is comparable to or less than the characteristic spacing of the scattering centers. The problem then becomes one of determining the criterion by which the magnetic

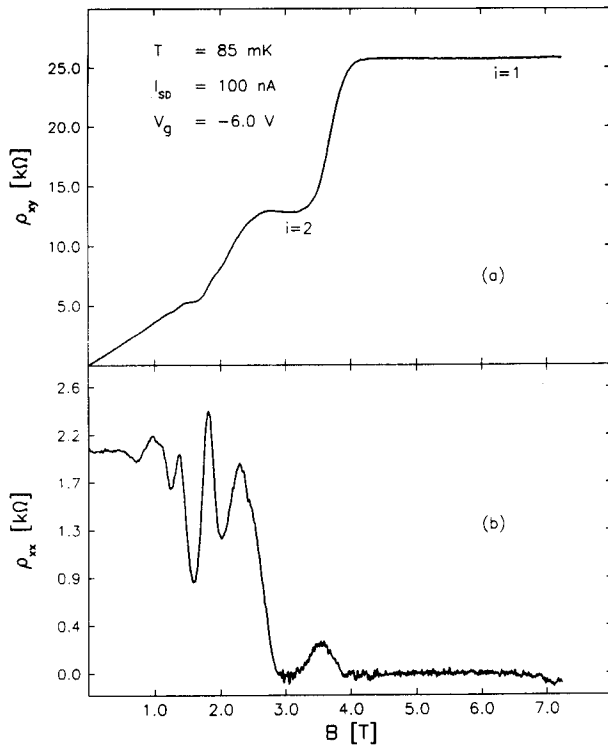


FIG. 5. (a) Hall resistance ρ_{xy} vs B for MCT with $n = 2.0 \times 10^{11} \text{ cm}^{-2}$. Plateaus corresponding to filling factor $i = 1$ and 2 are present in which $\rho_{xx} = 0$. (b) Corresponding diagonal magnetoresistance ρ_{xx} vs B for the sample at 85 mK.

length is less than or equal to the characteristic spacing of the randomly spaced scattering centers. This problem, then, is best handled by percolation theory. It can be shown that when the scattering centers, represented by a radius d , reach a concentration given by $n_{sc} = 0.35/(d + l/2)^2$ they will be closer spaced than the magnetic length of the extended states. At such point the QHE will not exist. If $d \ll l$ then this argument can be used to show that the critical field B_c for the onset of the QHE is given by

$$B_c = \frac{\hbar}{1.4e} n_{sc} \tag{1}$$

From Eq. (1) we have determined that the isotropic density of scattering centers in the MCT sample is $n_{sc} = 4.3 \times 10^{11} \text{ cm}^{-2}$. This number can then be compared with the fixed charge density n_{fc} obtained from CV measurements on the MCT, as shown in Fig. 6. In particular, we find $n_{fc} = 1.6 \times 10^{12} \text{ cm}^{-2}$. There is about a factor of 3 difference between n_{sc} and n_{fc} ; consequently, if the scattering centers arise from the fixed charges in the vicinity of the interface, then this implies some clustering and/or possibly some appreciable three-dimensional extent of the fixed charges. Thus the effective density of scattering centers experienced by the electrons in the inversion layer is less than the density of fixed charges. Clearly, we learn from this situation that the observation of the abrupt onset of the QHE provides a useful new way to gain some additional information about transport mechanisms in a 2-DEG.

Finally the MISFET structure allows us to make a simultaneous measurement of the MCT 2-DEG and the 2-DEG of

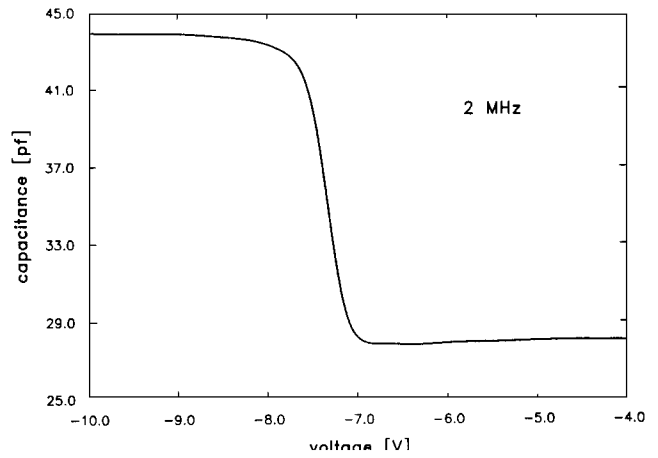


FIG. 6. CV measurement of MCT sample made at 2 MHz. Gate for this measurement was $254 \times 381 \mu\text{m}^2$ spaced above HgCdTe surface by a 800 \AA native oxide + 2000 \AA ZnS insulator.

the high mobility GaAs/AlGaAs heterostructure described above. In this case the MISFET and the heterostructure were connected in series to the current source. With the MISFET gate voltage adjusted to make the carrier density of the MCT nearly equal to that of the GaAs device, we are able to demonstrate explicitly the universality of the quantum Hall effect. The results are shown in Fig. 7. We find that the values of the Hall plateaus of each sample, corresponding to the $i = 2$ and 4 levels, agree to within 0.1% of each other and with the theoretical value, $\rho_{xy} = h/e^2 i$.

Also shown in Fig. 7 are circled regions indicating discontinuities in the MCT behavior. Presently our understanding of what causes these discontinuities is incomplete. However,

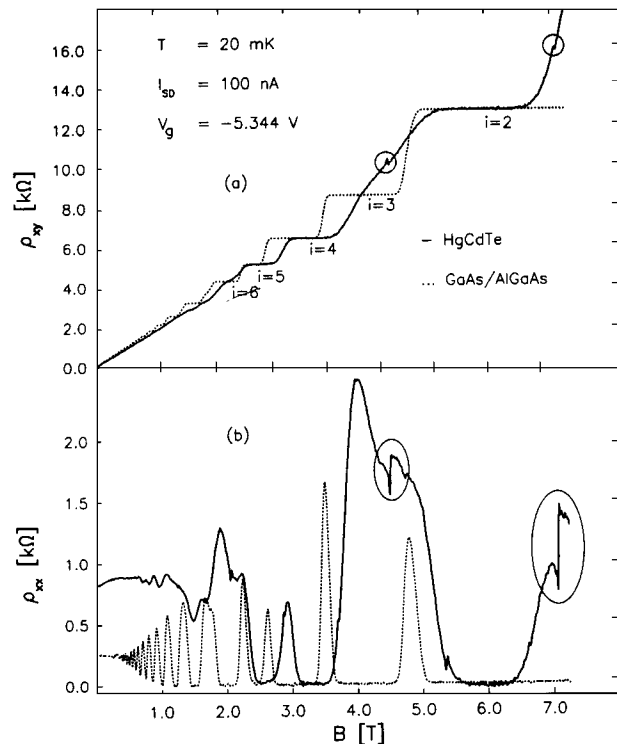


FIG. 7. (a) Direct comparison of MCT and GaAs/AlGaAs as a function of ρ_{xy} vs B . (b) Comparison of ρ_{xx} vs B for the two devices. Circled regions represent discontinuities in the MCT behavior (see the text).

we have demonstrated that their origin is not due to instrumental effects because the measurements were done simultaneously on the series-connected HgCdTe and GaAs samples. In addition, concurrent measurements of two Hall potentials and two longitudinal voltages were done using four digital voltmeters connected to the two probe sets shown in Fig. 1. These measurements displayed correlated behavior, i.e., the discontinuity features appeared concurrently in the Hall potentials from each probe set and in the longitudinal voltages from either side of the channel; hence this provided further evidence that the voltage contacts were performing as expected. We have also observed that the discontinuities depend on gate voltage (carrier density), amount of radiation exposure of the sample, and the excitation current. They also display some temporal effects on the order of minutes.

IV. SUMMARY

Through the use of a HgCdTe MISFET device we have clearly observed for the first time the existence of the quantum Hall effect in a type II–VI compound. Furthermore, we have presented new evidence for the abrupt onset of the QHE. This observation has allowed us to show that the application of the QHE can be effectively used to characterize the HgCdTe inversion layer. In particular, we calculated the number of scattering centers in a 2-DEG formed by the inversion layer. Moreover, the QHE promises to be a useful phenomena in general for characterizing transport proper-

ties in the 2-DEG of HgCdTe superlattices and for understanding properties of HgCdTe, as well as other types of semiconductor interfaces, where a two-dimensional electron gas may reside.

ACKNOWLEDGMENTS

We appreciate the assistance of Eric Palm in analyzing the data. Our special thanks go to Faye Carr for fabrication of the MCT sample, and to Hung-Dah Shih for growing the GaAs MBE sample. We also thank Bob Bate and Grady Roberts at TI for their encouraging support. We are grateful to the National Science Foundation–Low Temperature Program (DMR-8405197) for financial support.

¹K. von Klitzing, G. Dorda, and M. Pepper, *Phys. Rev. Lett.* **45**, 494 (1980).

²D. C. Tsui, H. L. Störmer, and A. C. Gossard, *Appl. Phys. Lett.* **38**, 550 (1981).

³H. L. Störmer, J. P. Eisenstein, A. C. Gossard, W. Wiegmann, and K. Baldwin, *Phys. Rev. Lett.* **56**, 85 (1986).

⁴S. G. Parker and H. Kraus, U.S. Patent No. 3 486 363 (1969).

⁵L. O. Bubulac, W. E. Tennant, S. H. Shin, C. C. Wang, M. Lanir, E. R. Gertner, and E. D. Marshall, *Jpn. J. Appl. Phys.* **19**, Suppl. 19-1, 495 (1980).

⁶R. A. Schiebel, *IEDM Tech. Dig.* **1983**, 711.

⁷D. C. Tsui and S. J. Allen, Jr., *Phys. Rev. B* **24**, 4082 (1981).

⁸R. Joynt and R. E. Prange, *Phys. Rev. B* **29**, 3303 (1984).